Available online at www.sciencedirect.com
ScienceDirect
Journal of Computational Physics 223 (2007) 846–864
JOURNAL OF COMPUTATIONAL PHYSICS
www.elsevier.com/locate/jcp

Extending the fast multipole method to charges inside or outside a dielectric sphere

Wei Cai [a,*], Shaozhong Deng [a], Donald Jacobs [b]

[a] Department of Mathematics and Statistics, University of North Carolina at Charlotte, Charlotte, NC 28223, United States
[b] Department of Physics and Optical Science, University of North Carolina at Charlotte, Charlotte, NC 28223, United States

Received 29 May 2006; received in revised form 22 September 2006; accepted 4 October 2006
Available online 1 December 2006

Abstract

In this paper, we propose a novel method to extend the fast multipole method (FMM) to calculate the electrostatic potential due to charges inside or outside a dielectric sphere. The key result which allows such an extension is the construction of a small number (two for a 10^{-2} relative error in reaction potentials inside the sphere) of image point charges for source point charges inside or outside the dielectric sphere. Numerical results validate the accuracy and high efficiency of the resulting algorithm.

AMS subject classifications: 65N38; 78M25

Keywords: Fast multipole method; Image charge; Dielectric sphere

1. Introduction

The fast multipole method (FMM) [1,2] has been recognized as one of the most significant recent algorithm developments with important scientific and engineering applications, such as electrostatic potential calculations [3], and fast solvers for integral equations for electromagnetic scattering [4,5]. The FMM relies on the analytical property of Green's functions for the Laplace operator for electrostatic potentials or the Helmholtz operator for wave scattering. Therefore, the FMM has only been used for the cases of homogeneous media or the situations where Green's functions can be obtained by methods of images for layered media [5]. In this paper, we propose a novel method to extend the FMM to the case of a dielectric sphere where source point charges are either inside or outside. The problem of finding the electrostatic potential for charges inside a spherical cavity with a dissimilar dielectric constant than the surrounding medium has applications in the study of quantum dots, and the calculation of the reaction field within a hybrid explicit/implicit spherical sol-

* Corresponding author. Tel.: +1 704 687 4581; fax: +1 704 687 6415.
E-mail address: wcai@uncc.edu (W. Cai).

0021-9991/$ - see front matter
doi:10.1016/j.jcp.2006.10.019

vation model for biomolecules such as proteins [6]. A fast algorithm of O(N) will have wide impact in computational simulations in many other areas, too.

An important development, which allows us to extend the FMM to the case of a dielectric sphere, is the construction of a small number of discrete images (two images for a 10^{-2} relative error and four images for a 10^{-4} relative error for most cases in reaction potentials inside the sphere) for charges inside or outside the sphere to approximate the potential field in the whole space. This construction is based on a result of over 100 year history dating back to Neumann in 1883 [7] and Lindell in 1994 [8–10], which extended the Kelvin image [11] for a conducting sphere to the case of a dielectric sphere. In the case of a dielectric sphere, in addition to an image point charge at the Kelvin image inverse point, there is an image line charge along a ray extending from the inverse point to infinity or to the center of the sphere depending on whether the source charge is inside or outside the sphere and where an observation point is located. Lindell has provided the power law distribution for the line charge density along the ray. To the knowledge of the authors, this elegant and incredible result has not been put into use in developing a numerical algorithm for calculating the potential field due to charges located inside or outside a dielectric sphere. It is noted that the calculation of potential fields for multiple closely spaced *conducting* cylinders and spheres has been addressed in [12,13] using a method of image charges. In this paper, we will develop specific methods to construct a small number of equivalent image point charges for a *dielectric* sphere, based on the image line charge results of Neumann/Lindell, and apply the FMM to calculate potentials in the whole space due to source point charges inside or outside the dielectric sphere.

The rest of this paper is organized as follows. In Section 2, we will briefly review the classical electrostatic theory to find the potential of a point charge inside or outside a dielectric sphere. In Section 3, we will first review the results of image line charges for point charges inside and outside a dielectric sphere with detailed derivations being provided for completeness in Appendix A. Then, we will show how to construct equivalent sets of discrete image point charges to represent the image line charges. Careful study of various choices of the discrete point charges (magnitudes and locations) is given. The smallest number of image point charges is provided for a given source charge location for a desired accuracy in the reaction potential. In Section 4, we will discuss how to apply the FMM to calculate the potential in the whole space due to source point charges. Numerical examples are given in Section 5 to demonstrate the accuracy of images and the efficiency of the FMM with the image point charges for potential calculation. Finally, a conclusion is given in Section 6.

2. The potential of a point charge and a dielectric sphere

In this section, we shall briefly describe the classical electrostatic theory to find the potential of a point charge inside or outside a dielectric sphere. In particular, we shall consider a dielectric sphere of radius a with dielectric constant ϵ_i, which is centered at the origin of coordinates and embedded in an infinite homogeneous medium of dielectric constant ϵ_o.

We will denote by $\mathbf{x}$ the physical location of a point in the space and x the distance of this point to the center of the dielectric sphere.

2.1. Point charge inside the dielectric sphere: $r_s < a$

Let us begin by considering the potential of a point charge q located on the x-axis inside the sphere at a distance r_s from the center of the sphere, see Fig. 1(a). With respect to a spherical coordinate system (r, ϕ, θ), it is well-known that, because of the azimuthal symmetry, the potential $V(r, \theta)$ at any field point F due to the point charge q can be expressed in terms of Legendre polynomials of $\cos\theta$.

More precisely, when the field point F is outside the sphere, i.e. $r \geqslant a$, since the potential must be zero at infinity, it should be of the form

$$V(r,\theta) = \sum_{n=0}^{\infty} \frac{A_n}{r^{n+1}} P_n(\cos\theta),$$

where $P_n(x)$, $n = 0, 1, 2, \ldots$, are Legendre polynomials.

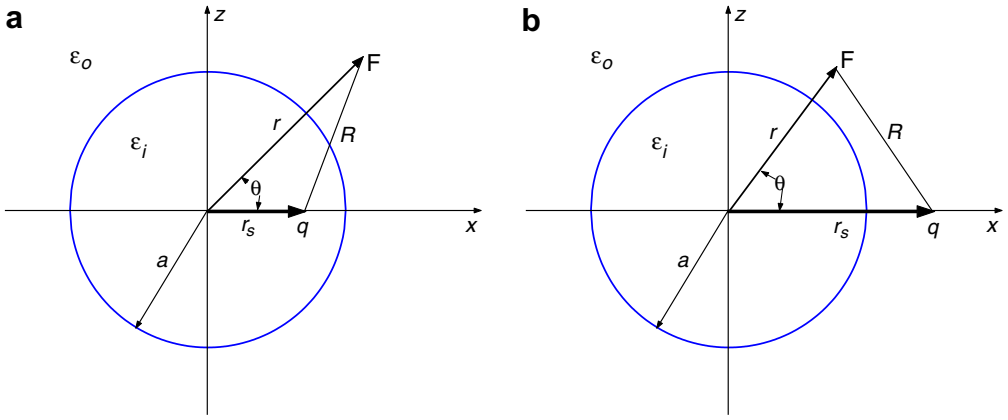

Fig. 1. A point charge and a dielectric sphere. (a) The point charge is inside the sphere ($r_s < a$); (b) The point charge is outside the sphere ($r_s > a$).

On the other hand, when the field point F is inside the sphere, i.e. $0 \leqslant r \leqslant a$, the potential due to the source point charge in a homogeneous medium is $q/(4\pi\epsilon_i R)$. We must superimpose on this a potential (*reaction potential*), due to the polarization of the dielectric, which must be finite at $r = 0$. Therefore, when $0 \leqslant r \leqslant a$, the total potential is

$$V(r,\theta) = \frac{q}{4\pi\epsilon_i R} + \sum_{n=0}^{\infty} B_n r^n P_n(\cos\theta). \tag{1}$$

Meanwhile, the potential due to the source point charge alone can also be expressed in terms of Legendre polynomials, see Appendix A.1. Depending on whether $r \geqslant r_s$ or $r \leqslant r_s$, we have

$$\frac{q}{4\pi\epsilon_i R} = \begin{cases} \dfrac{q}{4\pi\epsilon_i r} \displaystyle\sum_{n=0}^{\infty} \left(\frac{r_s}{r}\right)^n P_n(\cos\theta), & r_s \leqslant r \leqslant a, \\ \dfrac{q}{4\pi\epsilon_i r_s} \displaystyle\sum_{n=0}^{\infty} \left(\frac{r}{r_s}\right)^n P_n(\cos\theta), & 0 \leqslant r \leqslant r_s. \end{cases}$$

Hence, the potentials inside and outside the sphere take the form

$$V(r,\theta) = \begin{cases} \displaystyle\sum_{n=0}^{\infty} \frac{A_n}{r^{n+1}} P_n(\cos\theta), & a \leqslant r, \\ \displaystyle\sum_{n=0}^{\infty} \left[\frac{q}{4\pi\epsilon_i r}\left(\frac{r_s}{r}\right)^n + B_n r^n\right] P_n(\cos\theta), & r_s \leqslant r \leqslant a, \\ \displaystyle\sum_{n=0}^{\infty} \left[\frac{q}{4\pi\epsilon_i r_s}\left(\frac{r}{r_s}\right)^n + B_n r^n\right] P_n(\cos\theta), & 0 \leqslant r \leqslant r_s. \end{cases} \tag{2}$$

The expansion coefficients A_n and B_n in Eq. (2) are to be determined by the boundary conditions that the potentials are equal at the boundary of the sphere and the flux normal to the boundary is the same at either side of the boundary, i.e.

$$V(a^+,\theta) = V(a^-,\theta),$$
$$\epsilon_o \left.\frac{\partial V(r,\theta)}{\partial r}\right|_{r=a^+} = \epsilon_i \left.\frac{\partial V(r,\theta)}{\partial r}\right|_{r=a^-}.$$

Using the orthogonality of Legendre polynomials, we obtain

$$A_n = \frac{q}{4\pi\epsilon_i}\cdot\frac{r_s^n}{}\cdot\frac{1+\gamma}{2}\cdot\left(2+\frac{2\gamma}{1-\gamma+2n}\right),\quad n\geqslant 0, \tag{3}$$

$$B_n = \frac{q}{4\pi\epsilon_i}\cdot\frac{r_s^n}{a^{2n+1}}\cdot\gamma\cdot\left(1+\frac{1+\gamma}{1-\gamma+2n}\right),\quad n\geqslant 0, \tag{4}$$

where $\gamma=(\epsilon_i-\epsilon_o)/(\epsilon_i+\epsilon_o)$. Note that $\gamma=1$ corresponds to the case that the sphere is of infinite dielectric constant. Conversely, when $\gamma=-1$, the surrounding dielectric of the sphere is of infinite dielectric constant.

2.2. Point charge outside the dielectric sphere: $r_s > a$

Similarly, when the source point charge q is outside the dielectric sphere, as shown in Fig. 1(b), it can be readily shown that the potentials inside and outside the sphere take the form

$$V(r,\theta)=\begin{cases}\sum_{n=0}^{\infty} C_n r^n P_n(\cos\theta), & 0\leqslant r\leqslant a,\\ \sum_{n=0}^{\infty}\left[\frac{q}{4\pi\epsilon_o r_s}\left(\frac{r}{r_s}\right)^n+\frac{D_n}{r^{n+1}}\right]P_n(\cos\theta), & a\leqslant r\leqslant r_s,\\ \sum_{n=0}^{\infty}\left[\frac{q}{4\pi\epsilon_o r}\left(\frac{r_s}{r}\right)^n+\frac{D_n}{r^{n+1}}\right]P_n(\cos\theta), & r_s\leqslant r,\end{cases} \tag{5}$$

and the coefficients C_n and D_n in Eq. (5) are given by

$$C_n = \frac{q}{4\pi\epsilon_o}\cdot\frac{1}{r_s^{n+1}}\cdot\frac{1-\gamma}{2}\cdot\left(2+\frac{2\gamma}{1-\gamma+2n}\right),\quad n\geqslant 0, \tag{6}$$

$$D_n = -\frac{q}{4\pi\epsilon_o}\cdot\frac{a^{2n+1}}{r_s^{n+1}}\cdot\gamma\cdot\left(1-\frac{1-\gamma}{1-\gamma+2n}\right),\quad n\geqslant 0. \tag{7}$$

3. Charge images of a point charge and a dielectric sphere

3.1. Image line charges for a source point charge

In 1883, Carl Neumann gave an ingenious mathematical formulation of image line charges for a point charge inside or outside a dielectric sphere [7], effectively extending Kelvin's image charge of a point charge inside or outside a conducting sphere. Over one century later, these remarkable results had been rediscovered independently by Lindell [8–10] and Norris [14] in the 1990s. Below, we include in Table 1 the results in Norris's paper that give the magnitudes and the positions of various images. For completeness, we also include an appendix which contains the main derivation of these results (not available in Norris's paper).

In summary, in the case of an internal source point charge at $\mathbf{r}_s$, the reaction potential inside the sphere due to the polarization charges induced on the surface of the sphere is equal to the potential generated by an image

Table 1
Positions and magnitudes of image charges

	Position	Magnitude	Distributed image line charges
Internal source			
Interior field	$r_i\ (\geqslant a)$	$q'_{ii}=\gamma\frac{a}{r_s}q$	$q''_{ii}(x)=\frac{q}{a}\frac{\gamma(1+\gamma)}{2}\left(\frac{x}{r_i}\right)^{-\frac{1-\gamma}{2}},\quad r_i\leqslant x$
Exterior field	$r_s\ (\leqslant a)$	$q'_{io}=(1+\gamma)q$	$q''_{io}(x)=\frac{q}{r_s}\frac{\gamma(1+\gamma)}{2}\left(\frac{x}{r_s}\right)^{-\frac{1+\gamma}{2}},\quad 0\leqslant x\leqslant r_s$
External source			
Exterior field	$r_i\ (\leqslant a)$	$q'_{oo}=-\gamma\frac{a}{r_s}q$	$q''_{oo}(x)=\frac{q}{a}\frac{\gamma(1-\gamma)}{2}\left(\frac{x}{r_i}\right)^{-\frac{1+\gamma}{2}},\quad 0\leqslant x\leqslant r_i$
Interior field	$r_s\ (\geqslant a)$	$q'_{oi}=(1-\gamma)q$	$q''_{oi}(x)=\frac{q}{r_s}\frac{\gamma(1-\gamma)}{2}\left(\frac{x}{r_s}\right)^{-\frac{1-\gamma}{2}},\quad r_s\leqslant x$

Note. a is the radius of the sphere; r_s is the radial position of the source charge q; $r_i=a^2/r_s$ is the inverse point, and $\gamma=(\epsilon_i-\epsilon_o)/(\epsilon_i+\epsilon_o)$, $-1<\gamma<1$. The potential from the source point charge q at $\mathbf{r}_s$ will be added to the potential from the images for interior field points when q is inside the sphere, and for exterior field points when q is outside the sphere.

point charge q'_{ii} outside the sphere at the inverse point $\mathbf{r}_i = a^2\mathbf{r}_s/r_s^2$, and an image line charge that stretches from this inverse point to infinity with the charge distribution defined by $q''_{ii}(x)$. The potentials of these (point and line) image charges and of the original source charge must be added together to find the total potential field inside the sphere. Both the source and image charges are taken as acting in a homogeneous material of dielectric constant ϵ_i, which is that of the material of the sphere. On the other hand, the potential outside the sphere is equal to that from an image point charge q'_{io} at the location $\mathbf{r}_s$ of the source charge and an image line charge that stretches from the source point $\mathbf{r}_s$ inward to the center of the sphere with the charge distribution given by $q''_{io}(x)$.

Likewise, in the case of an external source point charge at $\mathbf{r}_s$, the reaction potential outside the sphere due to the charges induced on the surface of the sphere is equal to the potential generated by an image point charge q'_{oo} inside the sphere at the inverse point $\mathbf{r}_i$, and an image line charge that distributes from this inverse point inward to the center of the sphere with the line charge distribution defined by $q''_{oo}(x)$. The potentials of these (point and line) image charges and of the original source charge must be added together to find the total potential field outside the sphere. Both the source and image charges are taken as acting in a homogeneous material of dielectric constant ϵ_o, which is that of the surrounding material outside the sphere. On the other hand, the potential inside the sphere is equal to that from an image point charge q'_{oi} at the location $\mathbf{r}_s$ of the source charge and an image line charge that distributes from the source point $\mathbf{r}_s$ outward to infinity with the charge distribution given by $q''_{oi}(x)$.

3.2. Discrete image point charges for a source point charge

Within a given error tolerance in the potential field, we show how to construct an equivalent set of image point charges to represent the image line charges listed in Table 1. The basic idea is to transform the underlying line integral for the potential for an image line charge onto the finite interval $[-1,1]$, and then apply appropriate Gauss–Radau quadrature related to specific Jacobi polynomials. The resulting Jacobi–Gauss–Radau points and weights will give us magnitudes and locations of the desired discrete image point charges.

3.2.1. Source point charge inside the sphere: $r_s < a$

(a) The potential inside the sphereWe begin by considering how to accurately approximate the potential due to the image line charge $q''_{ii}(x)$, which stretches from the inverse point $\mathbf{r}_i$ to infinity, see Fig. 2(a). Recall from Section 3.1 that the total potential at a field point $F(\mathbf{r})$ inside the sphere, due to an internal point charge q, consists of three components: the potential $V_s(\mathbf{r};q)$ from the original source point charge q at $\mathbf{r}_s$, the potential $V_{ip}(\mathbf{r};q)$ from the image point charge q'_{ii} at the inverse point $\mathbf{r}_i$, and the potential $V_{il}(\mathbf{r};q)$ due to the distributed image line charge $q''_{ii}(x)$, i.e.

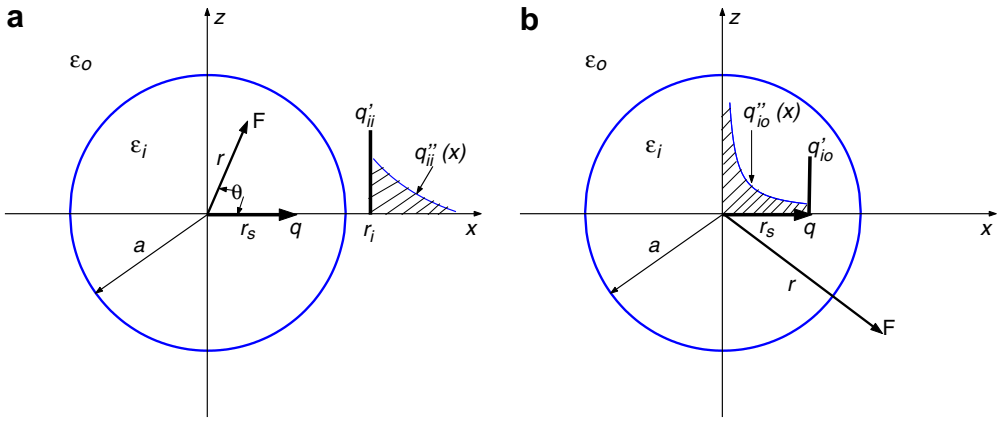

Fig. 2. Discretization of the image line charges $q''_{ii}(x)$ and $q''_{io}(x)$. (a) $q''_{ii}(x)$; (b) $q''_{io}(x)$.

$$V(\mathbf{r};q) = V_{\rm s}(\mathbf{r};q) + V_{\rm ip}(\mathbf{r};q) + V_{\rm il}(\mathbf{r};q) = \frac{q}{4\pi\epsilon_{\rm i}\cdot|\mathbf{r}-\mathbf{r}_{\rm s}|} + \frac{q'_{\rm ii}}{4\pi\epsilon_{\rm i}\cdot|\mathbf{r}-\mathbf{r}_{\rm i}|} + \int_{r_{\rm i}}^{\infty} \frac{q''_{\rm ii}(x)}{4\pi\epsilon_{\rm i}\cdot|\mathbf{r}-\mathbf{x}|}\,{\rm d}x, \tag{8}$$

where

$$r_{\rm i} = \frac{a^2}{r_{\rm s}}, \quad q'_{\rm ii} = \gamma\frac{a}{r_{\rm s}}q, \quad q''_{\rm ii}(x) = \frac{q}{a}\frac{\gamma(1+\gamma)}{2}\left(\frac{x}{r_{\rm i}}\right)^{-\frac{1-\gamma}{2}}, \quad r_{\rm i} \leqslant x.$$

One key to the success for the proposed extension of the FMM in Section 4 is to approximate, within a given error tolerance, the potential $V_{\rm il}(\mathbf{r};q)$ due to the image line charge $q''_{\rm ii}(x)$ by the potentials of a small number of discrete point charges. In order to achieve this, we discretize the following line integral by an appropriate numerical quadrature

$$I = \int_{r_{\rm i}}^{\infty} \frac{1}{|\mathbf{r}-\mathbf{x}|}\left(\frac{x}{r_{\rm i}}\right)^{-\frac{1-\gamma}{2}}{\rm d}x. \tag{9}$$

First, by introducing the change of variables $r_{\rm i}/x = ((1-s)/2)^{\tau}$ with $\tau > 0$, we have

$$I = \tau\cdot 2^{\frac{\gamma-1}{2}\tau}\int_{-1}^{1}(1-s)^{\alpha}\cdot h(\mathbf{r},s;\tau)\,{\rm d}s, \tag{10}$$

where $\alpha = (1-\gamma)\tau/2 - 1$ and

$$h(\mathbf{r},s;\tau) = \frac{2^{\tau}r_{\rm i}}{|(1-s)^{\tau}\mathbf{r} - 2^{\tau}\mathbf{r}_{\rm i}|}. \tag{11}$$

Next, we shall employ a numerical quadrature to approximate the integral I in Eq. (10). Note that $s=-1$ corresponds to the Kelvin image location $x = r_{\rm i}$. Also we have $\alpha > -1$ since $-1 < \gamma < 1$ and $\tau > 0$. Therefore, we can choose Gauss-Radau quadrature based on Jacobi polynomials. The Jacobi polynomials $P_n^{\alpha,\beta}(s)$ on the interval $[-1,1]$ are orthogonal polynomials under the Jacobi weight $w(s) = (1-s)^{\alpha}(1+s)^{\beta}$, i.e.

$$\int_{-1}^{1}(1-s)^{\alpha}(1+s)^{\beta}P_j^{\alpha,\beta}(s)P_k^{\alpha,\beta}(s)\,{\rm d}s = \delta_{jk},$$

where $\alpha > -1$, $\beta > -1$ [15]. More precisely, let s_m, ω_m, $m = 0,1,2,\ldots,M$ be the Jacobi–Gauss–Radau points and weights on the interval $[-1,1]$ with $s_0 = -1$ and $\alpha = (1-\gamma)\tau/2 - 1$, $\beta = 0$. Then, the numerical quadrature for approximating I in Eq. (10) is

$$I \approx \tau\cdot 2^{\frac{\gamma-1}{2}\tau}\sum_{m=0}^{M}\omega_m h(\mathbf{r},s_m;\tau), \tag{12}$$

which yields

$$V_{\rm il}(\mathbf{r};q) = \int_{r_{\rm i}}^{\infty}\frac{q''_{\rm ii}(x)}{4\pi\epsilon_{\rm i}\cdot|\mathbf{r}-\mathbf{x}|}\,{\rm d}x \approx \sum_{m=0}^{M}\frac{q_m^{\rm ii}}{4\pi\epsilon_{\rm i}\cdot|\mathbf{r}-\mathbf{x}_m^{\rm ii}|}, \tag{13}$$

where for $m = 0,1,2,\ldots,M$,

$$q_m^{\rm ii} = 2^{\frac{\gamma-1}{2}\tau-1}\gamma(1+\gamma)\tau\omega_m q\cdot\frac{x_m^{\rm ii}}{a}, \tag{14}$$

and

$$x_m^{\rm ii} = r_{\rm i}\cdot\left(\frac{2}{1-s_m}\right)^{\tau}. \tag{15}$$

Note that $x_0^{\rm ii} = r_{\rm i}$. Therefore, after combining together the point image charge $q'_{\rm ii}$ and the first discrete point charge $q_0^{\rm ii}$, we have an approximation of the total potential inside the sphere in terms of the potentials of $M+2$ point charges

$$V(\mathbf{r};q) \approx \frac{q}{4\pi\epsilon_i \cdot |\mathbf{r}-\mathbf{r}_s|} + \frac{q'_{ii}+q^{ii}_0}{4\pi\epsilon_i \cdot |\mathbf{r}-\mathbf{r}_i|} + \sum_{m=1}^{M} \frac{q^{ii}_m}{4\pi\epsilon_i \cdot |\mathbf{r}-\mathbf{x}^{ii}_m|}. \tag{16}$$

Remark 1 (*Three special cases*). The parameter $\tau > 0$ in the change of variables $r_i/x = ((1-s)/2)^\tau$ can be used as a parameter to control the accuracy of numerical approximation. When $\tau = 2/(1-\gamma)$ we have $\alpha = 0$, and in this case the quadrature given by Eq. (12) simply reduces to the Legendre–Gauss–Radau quadrature. When $\tau = 3/(1-\gamma)$, we have $\alpha = 1/2$. And when $\tau = 1/(1-\gamma)$, we have $\alpha = -1/2$.

Remark 2 (*Spacing analysis*). Assume that $s_M = 1 - O(1/M^2)$. Then $x^{ii}_M = O(M^{2\tau}) \cdot a^2/r_s$ is the farthest image point charge. A bigger τ will produce a bigger x^{ii}_M, which will consequently produce a bigger FMM cube in the FMM algorithm. Consider a few examples: In a typical biomolecular application where $\gamma \approx -1$, when $\tau = 3/(1-\gamma) \approx 3/2$, we will have $x^{ii}_M = O(M^3) \cdot a^2/r_s$; when $\tau = 2/(1-\gamma) \approx 1$ we will have $x^{ii}_M = O(M^2) \cdot a^2/r_s$; and when $\tau = 1/(1-\gamma) \approx 1/2$ we will have $x^{ii}_M = O(M) \cdot a^2/r_s$. Hence in terms of the size of the FMM cube, it seems that $\tau = 1/(1-\gamma)$ will be the best choice.

(b) The potential outside the sphere

As stated in Section 3.1, the total potential at a field point $F(\mathbf{r})$ outside the sphere due to an internal point charge q, see Fig. 2(b), consists of only two components: the potential $V_{ip}(\mathbf{r};q)$ from the image point charge q'_{io} at the same location $\mathbf{r}_s$ as the source charge, and the potential $V_{il}(\mathbf{r};q)$ due to the distributed image line charge $q''_{io}(x)$ stretching from $\mathbf{r}_s$ inward to the center of the sphere, i.e.

$$V(\mathbf{r};q) = V_{ip}(\mathbf{r};q) + V_{il}(\mathbf{r};q) = \frac{q'_{io}}{4\pi\epsilon_i \cdot |\mathbf{r}-\mathbf{r}_s|} + \int_0^{r_s} \frac{q''_{io}(x)}{4\pi\epsilon_i \cdot |\mathbf{r}-\mathbf{x}|}\,dx, \tag{17}$$

where

$$q'_{io} = (1+\gamma)q, \quad q''_{io}(x) = \frac{q}{r_s}\frac{\gamma(1+\gamma)}{2}\left(\frac{x}{r_s}\right)^{-\frac{1+\gamma}{2}}, \quad 0 \leqslant x \leqslant r_s.$$

Similarly, to construct an equivalent set of discrete image point charges for the image line charge $q''_{io}(x)$ within a given error tolerance, we need to approximate the following line integral by a numerical quadrature

$$I = \int_0^{r_s} \frac{1}{|\mathbf{r}-\mathbf{x}|}\left(\frac{x}{r_s}\right)^{-\frac{1+\gamma}{2}} dx. \tag{18}$$

After introducing the change of variables $x/r_s = ((1-s)/2)^\tau$ with $\tau > 0$, we obtain a similar integral as in Eq. (10) with

$$h(\mathbf{r},s;\tau) = \frac{2^\tau r_s}{|(1-s)^\tau \mathbf{r}_s - 2^\tau \mathbf{r}|}. \tag{19}$$

Therefore, for the same reason, we employ the numerical quadrature defined in Eq. (12) to approximate I in Eq. (18), yielding

$$V_{il}(\mathbf{r};q) = \int_0^{r_s} \frac{q''_{io}(x)}{4\pi\epsilon_i \cdot |\mathbf{r}-\mathbf{x}|}\,dx \approx \sum_{m=0}^{M} \frac{q^{io}_m}{4\pi\epsilon_i \cdot |\mathbf{r}-\mathbf{x}^{io}_m|}, \tag{20}$$

where for $m = 0, 1, 2, \ldots, M$,

$$q^{io}_m = 2^{\frac{\gamma-1}{2}\tau-1}\gamma(1+\gamma)\tau\omega_m q, \tag{21}$$

and

$$x^{io}_m = r_s \cdot \left(\frac{1-s_m}{2}\right)^\tau. \tag{22}$$

Note that $x_0^{\rm io} = r_{\rm s}$. Therefore, after combining together the point image charge $q'_{\rm io}$ and the first discrete point charge $q_0^{\rm io}$, we obtain an approximation of the total potential outside the sphere in terms of the potentials of $M+1$ point charges

$$V(\mathbf{r};q) \approx \frac{q'_{\rm io}+q_0^{\rm io}}{4\pi\epsilon_{\rm i}\cdot|\mathbf{r}-\mathbf{r}_{\rm s}|} + \sum_{m=1}^{M}\frac{q_m^{\rm io}}{4\pi\epsilon_{\rm i}\cdot|\mathbf{r}-\mathbf{x}_m^{\rm io}|}. \tag{23}$$

3.2.2. Source point charge outside the sphere: $r_s > a$

When the source point charge is outside the sphere, we can also construct equivalent discrete image point charges to the image line charges $q''_{\rm oo}(x)$ and $q''_{\rm oi}(x)$. As a matter of fact, after introducing similar changes of variables, we can transform the involving line integrals for the potentials from the image line charges into the same integral as in Eq. (10) but with a slightly different $h(\mathbf{r},s;\tau)$. Therefore, the same Jacobi–Gauss–Radau quadrature defined by Eq. (12) can be applied to find equivalent image point charges and their locations, which are summarized below.

(a) The potential outside the sphere

The total potential at a field point $F(\mathbf{r})$ outside the sphere due to an external point charge q consists of three components: the potential $V_{\rm s}(\mathbf{r};q)$ from the original source point charge q at $\mathbf{r}_{\rm s}$, the potential from the image point charge $q'_{\rm oo}$ at the inverse point $\mathbf{r}_{\rm i}$, and the potential due to the distributed image line charge $q''_{\rm oo}(x)$, i.e.

$$V(\mathbf{r};q) = \frac{q}{4\pi\epsilon_{\rm o}\cdot|\mathbf{r}-\mathbf{r}_{\rm s}|} + \frac{q'_{\rm oo}}{4\pi\epsilon_{\rm o}\cdot|\mathbf{r}-\mathbf{r}_{\rm i}|} + \int_0^{r_{\rm i}}\frac{q''_{\rm oo}(x)}{4\pi\epsilon_{\rm o}\cdot|\mathbf{r}-\mathbf{x}|}\,{\rm d}x, \tag{24}$$

where

$$q'_{\rm oo} = -\gamma\frac{a}{r_{\rm s}}q, \quad q''_{\rm oo}(x) = \frac{q}{a}\frac{\gamma(1-\gamma)}{2}\left(\frac{x}{r_{\rm i}}\right)^{-\frac{1+\gamma}{2}}, \quad 0 \leqslant x \leqslant r_{\rm i}.$$

The approximation of Eq. (24) in terms of $M+2$ equivalent image point charges is

$$V(\mathbf{r};q) \approx \frac{q}{4\pi\epsilon_{\rm o}\cdot|\mathbf{r}-\mathbf{r}_{\rm s}|} + \frac{q'_{\rm oo}+q_0^{\rm oo}}{4\pi\epsilon_{\rm o}\cdot|\mathbf{r}-\mathbf{r}_{\rm i}|} + \sum_{m=1}^{M}\frac{q_m^{\rm oo}}{4\pi\epsilon_{\rm o}\cdot|\mathbf{r}-\mathbf{x}_m^{\rm oo}|}, \tag{25}$$

where for $m = 0,1,2,\ldots,M$,

$$q_m^{\rm oo} = 2^{\frac{\gamma-1}{2}\tau-1}\gamma(1-\gamma)\tau\omega_m q\cdot\frac{a}{r_{\rm s}}, \tag{26}$$

and

$$x_m^{\rm oo} = r_{\rm i}\cdot\left(\frac{1-s_m}{2}\right)^{\tau}. \tag{27}$$

(b) The potential inside the sphere

The total potential at a field point $F(\mathbf{r})$ inside the sphere due to an external point source charge q consists of only two components: the potential from the image point charge $q'_{\rm oi}$ at the same location as the source charge $\mathbf{r}_{\rm s}$, and the potential due to the distributed image line charge $q''_{\rm oi}(x)$ stretching from $\mathbf{r}_{\rm s}$ outward to infinity, i.e.

$$V(\mathbf{r};q) = \frac{q'_{\rm oi}}{4\pi\epsilon_{\rm o}\cdot|\mathbf{r}-\mathbf{r}_{\rm s}|} + \int_{r_{\rm s}}^{\infty}\frac{q''_{\rm oi}(x)}{4\pi\epsilon_{\rm o}\cdot|\mathbf{r}-\mathbf{x}|}\,{\rm d}x, \tag{28}$$

where

$$q'_{\rm oi} = (1-\gamma)q, \quad q''_{\rm oi}(x) = \frac{q}{r_{\rm s}}\frac{\gamma(1-\gamma)}{2}\left(\frac{x}{r_{\rm s}}\right)^{-\frac{1-\gamma}{2}}, \quad r_{\rm s} \leqslant x.$$

The approximation of Eq. (28) in terms of $M+1$ equivalent image point charges is

$$V(\mathbf{r};q) \approx \frac{q'_{\rm oi}+q_0^{\rm oi}}{4\pi\epsilon_{\rm o}\cdot|\mathbf{r}-\mathbf{r}_{\rm s}|}+\sum_{m=1}^{M}\frac{q_m^{\rm oi}}{4\pi\epsilon_{\rm o}\cdot|\mathbf{r}-\mathbf{x}_m^{\rm oi}|}, \tag{29}$$

where for $m=0,1,2,\ldots,M$,

$$q_m^{\rm oi}=2^{\frac{\gamma-1}{2}\tau-1}\gamma(1-\gamma)\tau\omega_m q\cdot\frac{x_m^{\rm oi}}{r_{\rm s}}, \tag{30}$$

and

$$x_m^{\rm oi}=r_{\rm s}\cdot\left(\frac{2}{1-s_m}\right)^{\tau}. \tag{31}$$

For convenience, we list in Table 2 the magnitudes as well as the positions of all discrete image point charges for all four cases, where s_m, ω_m, $m=0,1,2,\ldots,M$ denote the Jacobi–Gauss–Radau points and weights on the interval $[-1,1]$ with the Jacobi weight $w(s)=(1-s)^{\alpha}(1+s)^{\beta}$, $\alpha=(1-\gamma)\tau/2-1$, and $\beta=0$. Both s_m and ω_m can be obtained with the program Orthpol [15].

4. Extending the FMM to dielectric spheres

With the approximation for the potentials by discrete point charges established, we are ready to extend the FMM to compute the potential involving a dielectric sphere. For instance, the procedures to evaluate the interior potential field due to point charges inside the sphere are as follows. All other cases can be done similarly.

(1) For each source point charge $q_{\rm s}$ at $\mathbf{r}_{\rm s}=(x_{\rm s},y_{\rm s},z_{\rm s})$ inside the sphere, find the corresponding point image $q'_{\rm ii}=(\gamma a/r_{\rm s})q_{\rm s}$ outside the sphere at the inverse point $\mathbf{r}_{\rm i}=a^2\mathbf{r}_{\rm s}/r_{\rm s}^2$, where $r_{\rm s}=(x_{\rm s}^2+y_{\rm s}^2+z_{\rm s}^2)^{1/2}$.
(2) In addition, for each source point charge $q_{\rm s}$ at $\mathbf{r}_{\rm s}=(x_{\rm s},y_{\rm s},z_{\rm s})$ inside the sphere, include $M+1$ discrete image point charges of magnitude

$$q_m^{\rm ii}=2^{\frac{\gamma-1}{2}\tau-1}\gamma(1+\gamma)\tau\omega_m q\cdot\frac{r_m^{\rm ii}}{a}, \tag{32}$$

at the location $\mathbf{r}_m^{\rm ii}=r_m^{\rm ii}\mathbf{r}_{\rm s}/r_{\rm s}$, where

$$r_m^{\rm ii}=\frac{a^2}{r_{\rm s}}\cdot\left(\frac{2}{1-s_m}\right)^{\tau}, \tag{33}$$

Table 2
Positions and magnitudes of discrete image point charges

	Magnitude	Position
Internal source		
Interior field	$q_m^{\rm ii}=2^{\frac{\gamma-1}{2}\tau-1}\gamma(1+\gamma)\tau\omega_m q\cdot\frac{x_m^{\rm ii}}{a}$	$x_m^{\rm ii}=r_{\rm i}\cdot(\frac{2}{1-s_m})^{\tau}$
Exterior field	$q_m^{\rm io}=2^{\frac{\gamma-1}{2}\tau-1}\gamma(1+\gamma)\tau\omega_m q$	$x_m^{\rm io}=r_{\rm s}\cdot(\frac{1-s_m}{2})^{\tau}$
		$m=0,1,2,\ldots,M$
External source		
Exterior field	$q_m^{\rm oo}=2^{\frac{\gamma-1}{2}\tau-1}\gamma(1-\gamma)\tau\omega_m q\cdot\frac{a}{x_m^{\rm ii}}$	$x_m^{\rm oo}=r_{\rm i}\cdot(\frac{1-s_m}{2})^{\tau}$
Interior field	$q_m^{\rm oi}=2^{\frac{\gamma-1}{2}\tau-1}\gamma(1-\gamma)\tau\omega_m q\cdot\frac{x_m^{\rm io}}{r_{\rm s}}$	$x_m^{\rm oi}=r_{\rm s}\cdot(\frac{2}{1-s_m})^{\tau}$
		$m=0,1,2,\ldots,M$

Note. s_m, ω_m, $m=0,1,2,\ldots,M$ are the Jacobi–Gauss–Radau points and weights on the interval $[-1,1]$ with $s_0=-1$ and $\alpha=(1-\gamma)\tau/2-1$, $\beta=0$. The potential from the source point charge q at $\mathbf{r}_{\rm s}$ will be added to the potential from the images for interior field points when q is inside the sphere, and for exterior field points when q is outside the sphere.

nd s_m, ω_m, $m = 0, 1, 2, \ldots, M$ are the Jacobi–Gauss–Radau points and weights on the interval $[-1, 1]$ ased on the Jacobi polynomial with $\alpha = (1-\gamma)\tau/2 - 1$, $\beta = 0$ and $\tau > 0$.

pply the FMM to calculate the potential by including all original point charges q_s, all point image harges q'_{ii}, and all discrete image point charges q_m^{ii} into the FMM cube, where all charges are taken s acting in a homogeneous medium of dielectric constant ϵ_i. (In the case that the source charges are out- ide the sphere, the dielectric constant outside the sphere ϵ_o will be used).

rk 3 (*Adaptive FMM*). It should be noted that, even though the original point charges could be rmly distributed inside or outside the sphere, image charges will be highly nonuniformly buted in a FMM cube. For instances, when evaluating interior fields due to internal sources, the bution of image charges outside the sphere will become sparser when moving away from the dary of the sphere. In contrast, when evaluating exterior fields due to the same internal sources, istribution of image charges inside the sphere will become denser when moving toward the center o phe 3. For reasons, an adaptive FMM [16–19] should be needed to achieve the enc

ark *ultipole sentation of all image charges*). In calculating the potential inside sphere g th tsid here, it is possible to convert all the potentials from those im charges in s o xpression at some point, say, the inverse point $\mathbf{r}_i$. As th ld inside the re p images can be considered in most cases far field, on few terms will need ress Similar arguments apply for the exterior field due images inside the ere. ve a smaller FMM cube and a smaller number total charges in the M gor approach will need a modification of the existi FMM code, which will essed

5 (*Direct ulat r very small r_s/a*). For source charges ry close to the center of the c sphere, th ma harges according to (33) will be fa way from the sphere boundary, in a large . Therefore, in this case, direct ca ation with series expansion (2) can where o s will be needed due to the fa convergence for small r_s. For instance, approac for $r_s/a < 0.01$, approximatel one millionth of uniformly distributed rges (see also Remark 4 for a rnative approach to reduce the size of the

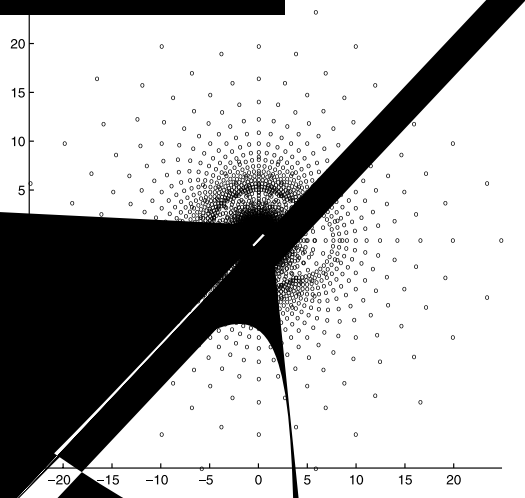

5. Numerical results

Due to the similarity of the analytical results for internal and external source point charges, we will only present here numerical results for the case that the charges are all inside the sphere. This case has considerable relevance in biophysical applications, as in biological structural analysis [6]. Unless otherwise specified, for demonstration purpose we assume all point charges are randomly but uniformly distributed in the region $0 \leqslant r \leqslant 0.9a$ inside the sphere with the magnitude of each point charge being either 1 or -1 such that the whole sphere is neutral. In addition, the radius of the sphere a is equal to 1, and the dielectric constants of the sphere and the surrounding medium are $\epsilon_i = 2$ and $\epsilon_o = 80$, respectively. Also, in this section NP represents the number of source point charges and NF represents the number of field points, respectively.

5.1. The number of image point charges vis the source location

As indicated earlier, the success of the proposed approach depends on whether the image line charges can be approximated, for a given error tolerance, by a small number of image point charges. To answer this question, we consider here one single point charge inside the sphere at a distance r_s away from the center of the sphere to investigate the dependence of the number of required discrete image point charges on the source location. When calculating the errors of the numerical approximation of the reaction potential, we use the results obtained with 200 Jacobi–Gauss–Radau points and $\tau = 2/(1-\gamma)$ as the "exact" values. Also, in the following table $\|E\|$ denotes the relative error in the reaction potential measured in L_∞ norm over all NF field points uniformly distributed on a cross-section through both the center of the sphere and the point charge, i.e.

$$\|E\| = \max_{1 \leqslant k \leqslant \mathrm{NF}} \left| \frac{V(\mathbf{x}_k) - \mathrm{EV}(\mathbf{x}_k)}{\mathrm{EV}(\mathbf{x}_k)} \right|,$$

where $\mathrm{EV}(\mathbf{x}_k)$ and $V(\mathbf{x}_k)$ denote the exact and the numerical reaction potential at a field point $\mathbf{x}_k$, respectively.

Table 3 lists the smallest number of image point charges needed to approximate reaction potential within a given error tolerance for different source locations. The listed results are for the case of $\tau = 3/(1-\gamma)$ only, but we have also tested the other two special cases $\tau = 1/(1-\gamma)$ and $\tau = 2/(1-\gamma)$. The two cases $\tau = 2/(1-\gamma)$ and $\tau = 3/(1-\gamma)$ have comparable accuracy, and both are better than the case of $\tau = 1/(1-\gamma)$. When calculating interior reaction fields, we use 100×100 field points uniformly distributed (under the polar coordinates) inside a unit disk. And when calculating exterior fields, we use 100×100 field points uniformly distributed (under the polar coordinates) inside a ring $a < r \leqslant 5a$. For example, from Table 3, we can conclude that when the source is located at $r_s = 0.5a$ away from the center of the sphere, 4 and 5 image point charges (including the Kelvin image charge) are needed for the approximation error to be less than 10^{-5} in relative errors when calculating the interior reaction fields and the exterior fields, respectively.

Table 3
Dependence of the number of image point charges on the source location

	r_s/a											
Interior fields												
$\|E\|$	0.01	0.1	0.2	0.3	0.4	0.5	0.6	0.7	0.8	0.9	0.95	0.99
10^{-2}	2	2	2	2	2	2	2	2	2	2	2	2
10^{-3}	2	2	2	2	2	2	2	3	3	3	4	5
10^{-4}	2	2	2	2	3	3	3	4	4	5	7	10
10^{-5}	2	2	3	3	3	4	4	5	6	8	10	17
10^{-6}	2	3	4	4	4	5	5	6	7	10	13	24
Exterior fields												
$\|E\|$	0.01	0.1	0.2	0.3	0.4	0.5	0.6	0.7	0.8	0.9	0.95	0.99
10^{-2}	2	2	2	2	2	2	3	3	3	4	4	5
10^{-3}	2	2	3	3	3	3	4	4	5	6	6	8
10^{-4}	2	3	3	3	4	4	4	5	6	7	9	11
10^{-5}	3	4	4	5	5	5	6	6	7	9	11	14
10^{-6}	4	5	5	7	7	7	8	8	9	11	13	17

As can be seen, only a small number of discrete images (less than 5 for most cases) are needed for 10^{-4} accuracy. In particular, when calculating interior reaction fields, two image charges are sufficient for the approximation error to be less than 1%, regardless of the source charge location. (If the Jacobi–Gauss quadrature is employed to construct discrete image charges, it has been found that three image charges are sufficient for the approximation error to be less than 0.1%, regardless of the source charge location.) For higher accuracy, unfortunately, more image point charges have to be used when the charge is close to the spherical boundary. As demonstrated in Section 5.2, compared with direct expansions, however, the proposed image method requires much less computations to achieve the same accuracy.

5.2. Comparison between the method of direct expansion and the method of images

It is well-known that when a charge is close to the boundary of the sphere, the convergence by direct series expansion (2) or (5) is slow, requiring a great number of terms to achieve high accuracy in the potential. Numerical experiments have shown that the method of direct expansion generally needs 50–70 terms to achieve the same order of accuracy as the method of images with only 4–5 equivalent image point charges (including the Kelvin image). Consequently, without using any acceleration strategy (like Ewald summations [20] for the method of direct expansion or the FMM for the method of images), the method of images generally is a factor of 20–30 times faster than the direct expansion approach. It is expected that this ratio will get larger as $r_s \to a$.

For example, Fig. 4(a) shows the approximation errors by direct expansion (2) when calculating interior fields due to NP randomly but uniformly distributed point charges in the region $r \leqslant 0.9a$ inside the sphere, while all NP field points are distributed randomly but uniformly inside the whole sphere. When calculating the errors of the numerical approximations, we use the results obtained by direct expansion with 200 terms as the "exact" values. Also, the relative error $||E||$ is measured in L_∞ norm over all NP observation points, i.e.

$$\|E\| = \frac{\max\limits_{1\leqslant k\leqslant \mathrm{NP}} |V(\mathbf{x}_k) - \mathrm{EV}(\mathbf{x}_k)|}{\max\limits_{1\leqslant k\leqslant \mathrm{NP}} |\mathrm{EV}(\mathbf{x}_k)|}, \tag{34}$$

where $\mathrm{EV}(\mathbf{x}_k)$ and $V(\mathbf{x}_k)$ denote the exact and the numerical total field potential at a field point $\mathbf{x}_k$, respectively. In this case, the approximation errors by the method of images with 4 image charges and $\tau = 1/(1-\gamma)$ are 1.97×10^{-5}, 5.15×10^{-5}, 6.09×10^{-5}, and 8.83×10^{-6} for NP = 6250, NP = 12,500, NP = 25,000, and NP = 50,000, respectively. It clearly shows that the direct expansion approach needs 50–70 terms to achieve the same order accuracy as the method of images.

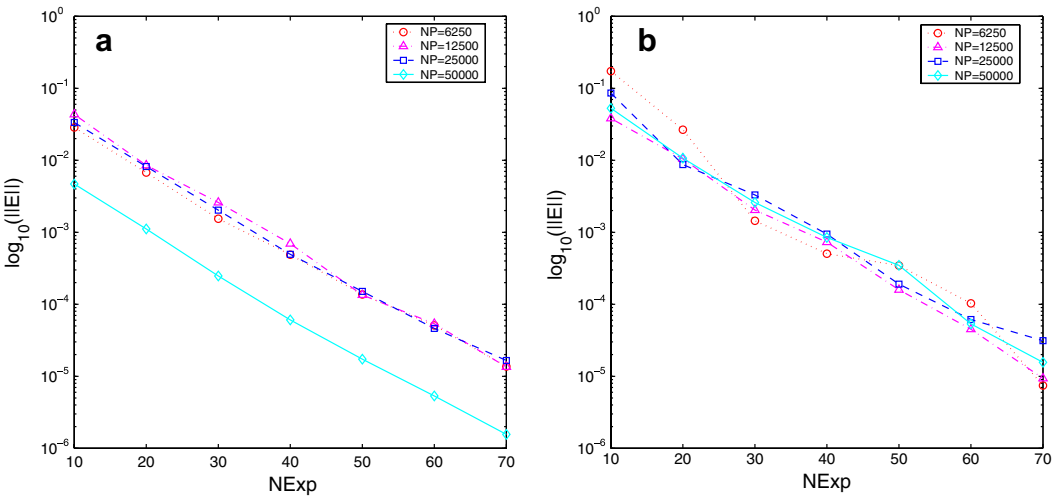

Fig. 4. Accuracy analysis results for the method of direct expansion, where *NExp* represents the number of used terms. (a) Results for interior fields; (b) results for exterior fields.

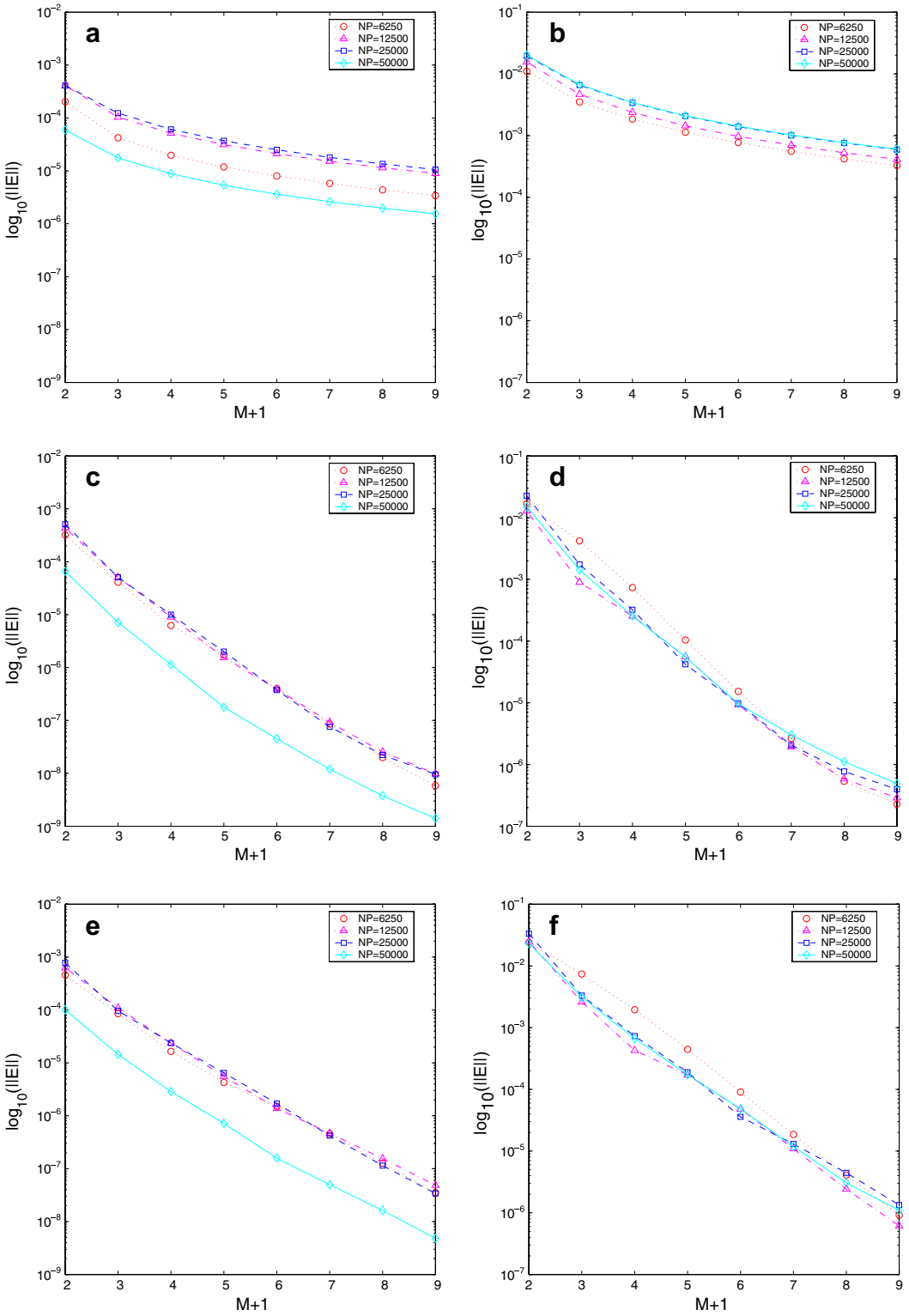

Fig. 5. Accuracy analysis results for the method of images. On the left panel are the results when calculating the interior fields, while on the right are those when calculating the exterior fields. (a, b) $\tau = 1/(1-\gamma)$; (c, d) $\tau = 2/(1-\gamma)$; and (e, f) $\tau = 3/(1-\gamma)$.

Table 4
CPU time in seconds on a 3 GHz-clock rate, 2GB-memory processor

NP	Interior fields			Exterior fields		
	NC	With FMM	No FMM	NC	With FMM	No FMM
6250	29,759	13.8	5.3	25,000	10.6	4.4
12,500	59,487	18.4	21.2	50,000	11.3	17.9
25,000	118,476	23.1	85.4	100,000	12.6	71.2
50,000	236,808	43.4	338.3	200,000	15.2	284.9

Similarly, Fig. 4(b) shows the approximation errors by direct expansion (5) when calculating exterior fields with the same set of internal point source charges. In this case, all NP field points are located in the region $a < r \leqslant 5a$ outside the sphere. The approximation errors by the method of images with 5 image charges and $\tau = 2/(1-\gamma)$ are 1.04×10^{-4}, 5.62×10^{-5}, 4.21×10^{-5}, and 5.56×10^{-5} for NP = 6250, NP = 12,500, NP = 25,000, and NP = 50,000, respectively. Again, it clearly indicates that the direct expansion approach needs 50–70 terms to achieve the same order accuracy as the method of images.

5.3. Accuracy of the method of images

In this section, we shall further investigate the dependence of the accuracy of the image method on the number of discrete image point charges. We only consider here the case that all NP point charges are inside the dielectric sphere.

Fig. 5 shows the error analysis results when we use images to calculate the total potentials inside and outside the sphere. First of all, it can be seen that for interior fields, only 3–4 discrete image point charges are needed to achieve 0.01% accuracy even for the worst choice of $\tau = 1/(1-\gamma)$. To achieve accuracy around 1%, only two image charges are needed! For exterior fields, even though the overall accuracy seems to be not as good as the interior field case, still only 5 image charges are needed to achieve 0.01% accuracy with $\tau = 2/(1-\gamma)$. Secondly, for both interior and exterior fields, the error analysis results seem to indicate that the accuracy for the case of $\tau = 2/(1-\gamma)$ (which corresponds to the Legendre–Gauss–Radau quadrature) is the best.

5.4. Field computation by the FMM

To investigate the efficiency of the method of images in conjunction with the FMM, the algorithm described in Section 4 has been implemented by using the free software *FastLap*, a general FMM-accelerated solver for Laplace problems developed by Professors Jacob K. White and Luca Daniel at MIT [3]. We assume that NP fields points are distributed randomly but uniformly inside the whole sphere or in the region $a < r \leqslant 5a$ outside the sphere, respectively. The experiments are carried out on a Dell OptiPlex GX280 workstation with a CPU clock rate of 3 GHz and a memory of 2 GB.

In Table 4, timing results of FMM calculation are reported and compared with those obtained without the FMM acceleration. The expansion order and the partitioning level in the FMM are set to be 2 and 9, respectively. To eliminate far point image charges, when calculating interior fields, we use direct summation of series expansion for charges near the center with $r_s < 0.1a$, i.e. 1 out of 1000 source point charges are treated by direct calculation (see Remark 5). For the same reason, when calculating interior fields, the number of image charges is adjusted based on how close a source point charge is to the boundary of the sphere. When calculating exterior fields, the number of image charges is set to be 4 for all source charges. As can be seen, the timing scales as $O(N^2)$ without the FMM acceleration, and linearly with the FMM. Note that in Table 4, NC denotes the number of total charges included in the FMM cube.

As the final remark, it should be noted that the software we employed, *FastLap*, is a general multipole-accelerated solver for Laplace problems. Therefore, it is possible to achieve better efficiency if we could develop a FMM solver specifically for field computation with our method of images. More importantly, since

the distribution of image charges are highly nonuniform, we believe much better efficiency can be achieved if an adaptive FMM is used.

6. Conclusion

In this paper, we have extended the FMM to calculating electrostatic potentials due to point charges inside or outside a dielectric sphere. Such an extension was made possible by constructing a small number of point image charges, based on a result of Neumann published in 1883, to approximate the potential accurately in the whole space. Numerical results have demonstrated the high accuracy of the images in approximating the potentials, and the high efficiency of using the FMM together with the constructed image charges to evaluate the resulting potentials. As the images constructed are not uniformly distributed, an adaptive FMM is preferred to achieve the best efficiency. As a further extension, a single pre-calculated multipole expansion can be derived to represent the potential produced by the image charges of a given source charge inside the sphere. These implementation improvements will be addressed in a future publication. Moreover, generalization of the image charge method to linearized Poisson-Boltzmann equations can also be done, which will be addressed in another future publication.

Acknowledgments

Wei Cai and Shaozhong Deng thank the support of the National Science Foundation (Grant Nos. DMS-0408309, CCF-0513179), the Department of Energy (Grant No. DEFG0205ER25678) and NERSC Computing Award, and Donald Jacobs thank the support from the National Institutes of Health (Grant No. NIGMS R01 GM073082-01A1), for the work reported in this paper. The authors also acknowledge the suggestion of one reviewer to use the Gauss–Radau quadrature, instead of our originally proposed Gauss quadrature, for the locations of the discrete images as presented in the final form of the paper.

Appendix A. Derivation of image charges of a point charge and a dielectric sphere

A.1. Harmonic expansion of the potential of a point charge in a homogeneous dielectric medium

Suppose that a point charge q is located on the z-axis at $z = d$, see Fig. 6. Then, it is well-known that the electric potential at a field point $F(\mathbf{r})$ generated by this single point charge equals to

$$V(\mathbf{r}) = \frac{q}{4\pi\epsilon R} = \frac{q}{4\pi\epsilon} \cdot \frac{1}{\sqrt{r^2 + d^2 - 2dr\cos\theta}}, \tag{A.1}$$

where R is the shortest distance between the point charge and the observation point F, θ is the angle between $\mathbf{d}$ and $\mathbf{r}$, and ϵ is the dielectric constant of the homogeneous medium.

If the radius r of the observation point F is greater than d, we may factor out $1/r$ and expand the square root in Eq. (A.1) in powers of $(d/r) < 1$ using Legendre polynomials $P_n(x)$

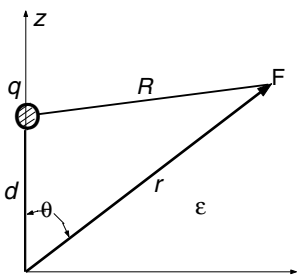

Fig. 6. Point charge in a homogeneous dielectric.

$$V(\mathbf{r}) = \frac{q}{4\pi\epsilon r}\sum_{n=0}^{\infty}\left(\frac{d}{r}\right)^n P_n(\cos\theta). \tag{A.2}$$

Conversely, if the radius r is less than d, we may factor out $1/d$ and expand the square root in Eq. (A.1) in powers of $(r/d) < 1$ using Legendre polynomials

$$V(\mathbf{r}) = \frac{q}{4\pi\epsilon d}\sum_{n=0}^{\infty}\left(\frac{r}{d}\right)^n P_n(\cos\theta). \tag{A.3}$$

A.2. Source point charge inside the sphere

A.2.1. Interior field

To obtain the potential inside the sphere due to the polarization, we plug the expansion coefficients B_n in Eq. (4) into Eq. (2) and obtain

$$\begin{aligned}\sum_{n=0}^{\infty} B_n r^n P_n(\cos\theta) &= \sum_{n=0}^{\infty}\frac{q}{4\pi\epsilon_{\mathrm{i}}}\cdot\frac{r_{\mathrm{s}}^n}{a^{2n+1}}\cdot\gamma\left(1+\frac{1+\gamma}{1-\gamma+2n}\right)r^n P_n(\cos\theta)\\ &= \frac{\gamma q}{4\pi\epsilon_{\mathrm{i}} r_{\mathrm{i}}}\frac{a}{r_{\mathrm{s}}}\sum_{n=0}^{\infty}\left(\frac{r}{r_{\mathrm{i}}}\right)^n P_n(\cos\theta)\\ &\quad + \frac{q}{4\pi\epsilon_{\mathrm{i}}}\frac{\gamma(1+\gamma)}{2}\sum_{n=0}^{\infty}\frac{r_{\mathrm{s}}^n}{a^{2n+1}}\cdot\frac{2}{1-\gamma+2n}\cdot r^n P_n(\cos\theta) = S_1 + S_2.\end{aligned}$$

The first part S_1 becomes exactly the expansion obtained from Eq. (A.3) by putting $d = r_{\mathrm{i}}$ and $\epsilon = \epsilon_{\mathrm{i}}$ for a point charge of magnitude

$$q'_{\mathrm{ii}} = \gamma\frac{a}{r_{\mathrm{s}}}q$$

outside the sphere at the inverse point $\mathbf{r}_{\mathrm{i}}$. For the second part, we note that

$$\int_{r_{\mathrm{i}}}^{\infty}\frac{1}{x^{\frac{1-\gamma}{2}+n+1}}\,\mathrm{d}x = \frac{2}{1-\gamma+2n}\cdot\left(\frac{1}{r_{\mathrm{i}}}\right)^{\frac{1-\gamma}{2}+n}.$$

Therefore, we have

$$\begin{aligned}S_2 &= \frac{q}{4\pi\epsilon_{\mathrm{i}}}\frac{\gamma(1+\gamma)}{2}\sum_{n=0}^{\infty}\left[\frac{a^{-\gamma}}{r_{\mathrm{s}}^{\frac{1-\gamma}{2}}}\int_{r_{\mathrm{i}}}^{\infty}\frac{1}{x^{\frac{1-\gamma}{2}+n+1}}\,\mathrm{d}x\right]r^n P_n(\cos\theta)\\ &= \int_{r_{\mathrm{i}}}^{\infty}\left[\frac{q}{4\pi\epsilon_{\mathrm{i}}x}\frac{1}{a}\frac{\gamma(1+\gamma)}{2}\left(\frac{x}{r_{\mathrm{i}}}\right)^{-\frac{1-\gamma}{2}}\sum_{n=0}^{\infty}\left(\frac{r}{x}\right)^n P_n(\cos\theta)\right]\mathrm{d}x\\ &= \int_{r_{\mathrm{i}}}^{\infty}\left[\frac{q''_{\mathrm{ii}}(x)}{4\pi\epsilon_{\mathrm{i}}x}\sum_{n=0}^{\infty}\left(\frac{r}{x}\right)^n P_n(\cos\theta)\right]\mathrm{d}x.\end{aligned}$$

Putting $d = x$ and $\epsilon = \epsilon_{\mathrm{i}}$ in Eq. (A.3), we can see that the inside of the above integral physically represents the potential generated by charge $q''_{\mathrm{ii}}(x)$ at $\mathbf{x}$, where

$$q''_{\mathrm{ii}}(x) = \frac{q}{a}\frac{\gamma(1+\gamma)}{2}\left(\frac{x}{r_{\mathrm{i}}}\right)^{-\frac{1-\gamma}{2}}, \quad r_{\mathrm{i}} \leqslant x.$$

A.2.2. Exterior field

Substituting the expansion coefficients A_n in Eq. (3) into Eq. (2), we have the potential in the region outside the sphere

$$\sum_{n=0}^{\infty}\frac{A_n}{r^{n+1}}P_n(\cos\theta)=\sum_{n=0}^{\infty}\frac{qr_s^n}{4\pi\epsilon_i}\cdot\frac{1+\gamma}{2}\cdot\left(2+\frac{2\gamma}{1-\gamma+2n}\right)\frac{1}{r^{n+1}}P_n(\cos\theta)$$
$$=\frac{(1+\gamma)q}{4\pi\epsilon_i r}\sum_{n=0}^{\infty}\left(\frac{r_s}{r}\right)^n P_n(\cos\theta)$$
$$+\frac{q}{4\pi\epsilon_i r}\frac{\gamma(1+\gamma)}{2}\sum_{n=0}^{\infty}\frac{2}{1-\gamma+2n}\cdot\left(\frac{r_s}{r}\right)^n P_n(\cos\theta)=S_1+S_2.$$

The first series S_1 is exactly the expansion obtained from Eq. (A.2) by putting $d=r_s$ and $\epsilon=\epsilon_i$ for a point charge of magnitude

$$q'_{io}=(1+\gamma)q$$

at the same location as the source charge. For the second series S_2, first we note that

$$\int_0^{r_s}x^{\frac{1-\gamma}{2}+n-1}\,dx=\frac{2}{1-\gamma+2n}\cdot(r_s)^{\frac{1-\gamma}{2}+n}.$$

Then, we can rewrite the second series S_2 as

$$S_2=\frac{q}{4\pi\epsilon_i r}\frac{\gamma(1+\gamma)}{2}\sum_{n=0}^{\infty}\left[(r_s)^{-\frac{1-\gamma}{2}}\int_0^{r_s}x^{\frac{1-\gamma}{2}+n-1}\,dx\right]\frac{1}{r^n}P_n(\cos\theta)$$
$$=\int_0^{r_s}\left[\frac{q}{4\pi\epsilon_i r}\frac{1}{r_s}\frac{\gamma(1+\gamma)}{2}\left(\frac{x}{r_s}\right)^{-\frac{1+\gamma}{2}}\sum_{n=0}^{\infty}\left(\frac{x}{r}\right)^n P_n(\cos\theta)\right]dx$$
$$=\int_0^{r_s}\left[\frac{q''_{io}(x)}{4\pi\epsilon_i r}\sum_{n=0}^{\infty}\left(\frac{x}{r}\right)^n P_n(\cos\theta)\right]dx.$$

Now it is easy to see, by putting $d=x$ and $\epsilon=\epsilon_i$ in Eq. (A.2), that the inside of the above integral represents the potential generated by a point charge $q''_{io}(x)$ at $\mathbf{x}$, where

$$q''_{io}(x)=\frac{q}{r_s}\frac{\gamma(1+\gamma)}{2}\left(\frac{x}{r_s}\right)^{-\frac{1+\gamma}{2}},\quad x\leqslant r_s.$$

A.3. Source point charge outside the sphere

A.3.1. Exterior field

To calculate the potential in the region outside the sphere in the presence of an external point charge, we plug the expansion coefficients D_n is Eq. (7) into Eq. (5) and obtain

$$\sum_{n=0}^{\infty}\frac{D_n}{r^{n+1}}P_n(\cos\theta)=-\sum_{n=0}^{\infty}\frac{q}{4\pi\epsilon_o}\frac{a^{2n+1}}{r_s^{n+1}}\gamma\left(1-\frac{1-\gamma}{1-\gamma+2n}\right)\frac{1}{r^{n+1}}P_n(\cos\theta)$$
$$=-\frac{\gamma q}{4\pi\epsilon_o r}\frac{a}{r_s}\sum_{n=0}^{\infty}\left(\frac{r_i}{r}\right)^n P_n(\cos\theta)$$
$$+\frac{q}{4\pi\epsilon_o r}\frac{\gamma(1-\gamma)}{2}\sum_{n=0}^{\infty}\frac{a^{2n+1}}{r_s^{n+1}}\cdot\frac{2}{1-\gamma+2n}\cdot\frac{1}{r^n}P_n(\cos\theta)=S_1+S_2.$$

If we let $d=r_i$ and $\epsilon=\epsilon_o$ in Eq. (A.2), then we can see clearly that the first series S_1 corresponds to the expansion of the potential due to a point charge of magnitude

$$q'_{oo}=-\gamma\frac{a}{r_s}q$$

inside the sphere at the inverse point $\mathbf{r}_i$. For the second series S_2, similarly noting that

$$\int_0^{r_i}x^{\frac{1-\gamma}{2}+n-1}\,dx=\frac{2}{1-\gamma+2n}\cdot(r_i)^{\frac{1-\gamma}{2}+n},$$

we have

$$S_2 = \frac{q}{4\pi\epsilon_o r}\frac{\gamma(1-\gamma)}{2}\sum_{n=0}^{\infty}\left[\left(\frac{r_s^{-\frac{1+\gamma}{2}}}{a^{-\gamma}}\right)\int_0^{r_i} x^{\frac{1-\gamma}{2}+n-1}\,dx\right]\frac{1}{r^n}P_n(\cos\theta)$$
$$= \int_0^{r_i}\left[\frac{q}{4\pi\epsilon_o r}\frac{1}{a}\frac{\gamma(1-\gamma)}{2}\left(\frac{x}{r_i}\right)^{-\frac{1+\gamma}{2}}\sum_{n=0}^{\infty}\left(\frac{x}{r}\right)^n P_n(\cos\theta)\right]dx$$
$$= \int_0^{r_i}\left[\frac{q''_{oo}(x)}{4\pi\epsilon_o r}\sum_{n=0}^{\infty}\left(\frac{x}{r}\right)^n P_n(\cos\theta)\right]dx.$$

Likely, if we let $d = x$ and $\epsilon = \epsilon_o$ in Eq. (A.2), we can see that the inside of the above integral physically represents the potential generated by a point charge $q''_{oo}(x)$ at $\mathbf{x}$ with

$$q''_{oo}(x) = \frac{q}{a}\frac{\gamma(1-\gamma)}{2}\left(\frac{x}{r_i}\right)^{-\frac{1+\gamma}{2}}, \quad 0 \leqslant x \leqslant r_i.$$

A.3.2. Interior field

Finally, plugging the expansion coefficients C_n in Eq. (6) into Eq. (5), we have the potential inside the sphere

$$\sum_{n=0}^{\infty} C_n r^n P_n(\cos\theta) = \sum_{n=0}^{\infty}\frac{q}{4\pi\epsilon_o}\frac{1}{r_s^{n+1}}\frac{1-\gamma}{2}\left(2+\frac{2\gamma}{1-\gamma+2n}\right)\cdot r^n P_n(\cos\theta)$$
$$= \frac{(1-\gamma)q}{4\pi\epsilon_o r_s}\sum_{n=0}^{\infty}\left(\frac{r}{r_s}\right)^n P_n(\cos\theta)$$
$$+\frac{q}{4\pi\epsilon_o r_s}\frac{\gamma(1-\gamma)}{2}\sum_{n=0}^{\infty}\frac{2}{1-\gamma+2n}\cdot\left(\frac{r}{r_s}\right)^n P_n(\cos\theta) = S_1 + S_2.$$

The first part S_1 becomes exactly the expansion given by Eq. (A.3) for a point charge of magnitude

$$q'_{oi} = (1-\gamma)q$$

at the same location as the source point charge. On the other hand, by using the fact that

$$\int_{r_s}^{\infty}\frac{1}{x^{\frac{1-\gamma}{2}+n+1}}\,dx = \frac{2}{1-\gamma+2n}\cdot\frac{1}{r_s^{\frac{1-\gamma}{2}+n}},$$

we can rewrite the second part S_2 as

$$S_2 = \frac{q}{4\pi\epsilon_o r_s}\frac{\gamma(1-\gamma)}{2}\sum_{n=0}^{\infty}\left[r_s^{\frac{1-\gamma}{2}}\int_{r_s}^{\infty}\frac{1}{x^{\frac{1-\gamma}{2}+n+1}}\,dx\right]r^n P_n(\cos\theta)$$
$$= \int_{r_s}^{\infty}\left[\frac{q}{4\pi\epsilon_o x}\frac{1}{r_s}\frac{\gamma(1-\gamma)}{2}\left(\frac{r_s}{x}\right)^{\frac{1-\gamma}{2}}\sum_{n=0}^{\infty}\left(\frac{r}{x}\right)^n P_n(\cos\theta)\right]dx$$
$$= \int_{r_s}^{\infty}\left[\frac{q''_{oi}(x)}{4\pi\epsilon_o x}\sum_{n=0}^{\infty}\left(\frac{r}{x}\right)^n P_n(\cos\theta)\right]dx.$$

The inside of the above integral is the same as the expansion obtained by putting $d = x$ and $\epsilon = \epsilon_o$ in Eq. (A.3) for a point charge q''_{oi} at $\mathbf{x}$, where

$$q''_{oi}(x) = \frac{q}{r_s}\frac{\gamma(1-\gamma)}{2}\left(\frac{x}{r_s}\right)^{-\frac{1-\gamma}{2}}, \quad r_s \leqslant x.$$

References

[1] L. Greengard, V. Rokhlin, A fast algorithm for particle simulations, J. Comput. Phys. 73 (1987) 325–348.
[2] L. Greengard, The Rapid Evaluation of Potential Fields in Particle Systems, MIT, Cambridge, 1987.
[3] K. Nabors, J. White, Fastcap: A multipole accelerated 3D capacitance extraction program, IEEE Trans. CAD 10 (1991) 1447–1459.
[4] W.C. Chew, Fast algorithms for wave scattering developed at the University of Illinois' Electromagnetics Laboratory, IEEE Antenn. Propag. Mag. 35 (1993) 22–32.
[5] Y.C. Pan, W.C. Chew, L.X. Wan, A fast multipole method based calculation of the capacitance matrix for multiple conductors above stratified media, IEEE Trans. Microw. Theory Tech. 49 (2001) 480–490.
[6] A. Okur, C. Simmerling, Hybrid explicit/implicit solvation methods, in: David Spellmeyer (Ed.), Annual Reports in Computational Chemistry, vol. 2, 2006 (Chapter 6).
[7] C. Neumann, Hydrodynamische Untersuchen nebst einem Anhang uber die Probleme der Elecktrostatik und der magnetischen Induktion, Teubner, Leipzig, 1883, pp. 279–282.
[8] I.V. Lindell, Electrostatic image theory for the dielectric sphere, Radio Sci. 27 (1992) 1–8.
[9] I.V. Lindell, M.E. Ermutlu, A.H. Sihvola, Electrostatic image theory for layered dielectric sphere, IEE Proc.-H 139 (1992) 186–192.
[10] I.V. Lindell, Image theory for electrostatic and magnetostatic problems involving a material sphere, Am. J. Phys. 61 (1993) 39–44.
[11] J.D. Jackson, Classical Electrodynamics, John Wiley, New York, 1999.
[12] H.W. Cheng, L. Greengard, A method of images for the evaluation of electrostatic fields in systems of closely spaced conducting cylinders, SIAM J. Appl. Math. 58 (1998) 122–141.
[13] H.W. Cheng, On the method of images for systems of closely spaced conducting spheres, SIAM J. Appl. Math. 61 (2000) 1324–1337.
[14] W.T. Norris, Charge images in a dielectric sphere, IEE Proc.-Sci. Meas. Technol. 142 (1995) 142–150.
[15] W. Gautschi, Algorithm 726; ORTHPOL a package of routines for generating orthogonal polynomials and Gauss-type quadrature rules, ACM Trans. Math. Softw. 20 (1994) 21–62.
[16] J. Carrier, L. Greengard, V. Rokhlin, A fast adaptive multipole algorithm for particle simulations, SIAM J. Sci. Stat. Comput. 9 (1988) 669–686.
[17] K. Nabors, T. Korsmeyer, J. White, Preconditioned, adaptive, multipole-accelerated iterative methods for three-dimensional first-kind integral equations of potential theory, SIAM J. Sci. Comput. 15 (1994) 713–735.
[18] H. Cheng, L. Greengard, V. Rokhlin, A fast adaptive multipole algorithm in three dimensions, J. Comput. Phys. 155 (1999) 468–498.
[19] J.P. Singh, C. Holt, J.L. Hennessy, A. Gupta, A parallel adaptive fast multipole method, in: Proceedings of the 1993 ACM/IEEE Conference on Supercomputing, Portland, Oregon, United States, 1993, pp. 54–65.
[20] T. Darden, D. York, L. Pedersen, Particle mesh Ewald: an $n\log n$ method for Ewald sums in large systems, J. Chem. Phys. 99 (1993) 10089–10092.